Supplement of

Assessment of smoke plume height products derived from multisource satellite observations for wildfire in the western US

Jingting Huang et al.

Correspondence to: Jingting Huang (jingting.huang@utah.edu)

Table S1: Location and elevation of balloon sounding stations near the UWKA flight operations during the August 2018 BB-FLUX project.

Station ID	Latitude	Longitude	Elevation (m AMSL)
BOI	43.56	-116.21	874
LKN	40.86	-115.73	1608
MFR	42.36	-122.86	405
SLC	40.77	-111.95	1289

Table S2: Physical schemes used in the WRF simulations. A 4-km domain across the western U.S. with a domain size of 629 × 501 (east-west direction × north-south direction) in the WRF configuration is centered at (40° N,116° W).

Physical Process	Scheme
Microphysics	Purdue Lin Scheme (Chen and Sun, 2002)
Convection	Grell–Devenyi Ensemble Scheme (Grell and Dévényi, 2002)
Short/Long-wave radiation	RRTMG Shortwave and Longwave Schemes (Iacono et al., 2008)
Planetary boundary layer	Yonsei University scheme (Hong et al., 2006)
Surface layer	Revised MM5 Scheme (Jiménez et al., 2012)
Land surface	Unified Noah Land Surface Model (Mukul Tewari et al., 2004)

Table S3: Statistical evaluation of satellite-retrieved wildfire *SPH* products against WCL-determined *SPH* observations using the spatial averaging method. *N* – the number of collocated pairs; *STD* – standard deviation; *Q25* – lower quartile, 25% of the data lie below this value; *Q50* – median, 50% of the data lie below this value; *Q75* – upper quartile, 25% of the data lie above this value; *MB* – mean bias; *MAE* – mean absolute error; *RMSE* – root mean square error; *r* – Pearson's correlation coefficient score.

	WCL-Determined *SPH*	
	SPH^{top}	SPH^{ext}
MODIS-Terra/MAIAC		
N	163	
Lidar Observations Mean ± 1 *STD* (km)	2.162 ± 0.542	1.382 ± 0.368
Satellite Retrievals Mean ± 1 *STD* (km)	0.733 ± 0.447	
Lidar Observations $^{Max}/_{Min}$ (km)	$^{3.903}/_{1.254}$	$^{2.253}/_{0.800}$
Satellite Retrievals $^{Max}/_{Min}$ (km)	$^{2.114}/_{0.015}$	
Lidar Observations *Q25*, *Q50*, *Q75* (km)	1.776, 2.064, 2.508	1.131, 1.298, 1.581
Satellite Retrievals *Q25*, *Q50*, *Q75* (km)	0.438, 0.687, 0.903	
MB (km)	-1.429	-0. 650
MAE (km)	1.429	0.673
RMSE (km)	1.591	0.822
r	0.008	**0.247** **
MODIS-Aqua/MAIAC		
N	114	
Lidar Observations Mean ± 1 *STD* (km)	2.686 ± 0.797	1.790 ± 0.644

Satellite Retrievals Mean ± 1 *STD* (km)	0.425 ± 0.262	
Lidar Observations $^{Max}/_{Min}$ (km)	$^{4.215}/_{1.374}$	$^{3.422}/_{0.800}$
Satellite Retrievals $^{Max}/_{Min}$ (km)	$^{0.935}/_{0.025}$	
Lidar Observations *Q25*, *Q50*, *Q75* (km)	2.063, 2.627, 3.350	1.274, 1.728, 2.325
Satellite Retrievals *Q25*, *Q50*, *Q75* (km)	0.192, 0.379, 0.697	
MB (km)	-2.261	-1.365
MAE (km)	2.261	1.365
RMSE (km)	2.393	1.525
r	**0.219** *	0.057
MISR/MERLIN		
N	90	
Lidar Observations Mean ± 1 *STD* (km)	2.216 ± 0.506	1.498 ± 0.449
Satellite Retrievals Mean ± 1 *STD* (km)	2.124 ± 0.625	
Lidar Observations $^{Max}/_{Min}$ (km)	$^{2.982}/_{1.254}$	$^{2.253}/_{0.853}$
Satellite Retrievals $^{Max}/_{Min}$ (km)	$^{3.029}/_{0.625}$	
Lidar Observations *Q25*, *Q50*, *Q75* (km)	1.791, 2.204, 2.648	1.129, 1.428, 1.969
Satellite Retrievals *Q25*, *Q50*, *Q75* (km)	1.658, 2.083, 2.801	
MB (km)	-0.092	0. 626
MAE (km)	0.368	0.719
RMSE (km)	0.554	0.788
r	**0.551** **	**0.648** **
VIIRS/ASHE		
N	130	
Lidar Observations Mean ± 1 *STD* (km)	2.823 ± 0.999	1.895 ± 0.890
Satellite Retrievals Mean ± 1 *STD* (km)	2.707 ± 1.149	
Lidar Observations $^{Max}/_{Min}$ (km)	$^{5.493}/_{1.497}$	$^{4.003}/_{0.811}$
Satellite Retrievals $^{Max}/_{Min}$ (km)	$^{4.603}/_{0.227}$	
Lidar Observations *Q25*, *Q50*, *Q75* (km)	1.977, 2.904, 3.318	1.094, 1.629, 2.489
Satellite Retrievals *Q25*, *Q50*, *Q75* (km)	2.263, 2.6661, 3.625	
MB (km)	-0.106	0.823
MAE (km)	1.196	1.599
RMSE (km)	1.694	1.814
r	**-0.236** *	**-0.246** *
TROPOMI/ALH		
N	127	
Lidar Observations Mean ± 1 *STD* (km)	2.677 ± 1.075	1.894 ± 0.936
Satellite Retrievals Mean ± 1 *STD* (km)	2.001 ± 0.541	
Lidar Observations $^{Max}/_{Min}$ (km)	$^{5.493}/_{1.374}$	$^{4.003}/_{0.734}$
Satellite Retrievals $^{Max}/_{Min}$ (km)	$^{3.425}/_{1.412}$	

Lidar Observations *Q25*, *Q50*, *Q75* (km)	1.718, 2.337, 3.308	1.019, 1.542, 2.684
Satellite Retrievals *Q25*, *Q50*, *Q75* (km)	1.546, 1.759, 2.391	
MB (km)	-0.676	0.107
MAE (km)	0.850	0.843
RMSE (km)	1.324	0.980
r	0.130	**0.218** *

*Note that the Pearson's correlation coefficient scores (r) in bold demonstrate a statistically significant relationship between the two variables; the symbol * signifies a p value < 0.05 and ** indicates a p value < 0.01. A lower p-value suggests a higher level of statistical significance.*

Table S4: Statistical evaluation of satellite-retrieved wildfire *SPH* products against WCL-determined *SPH* observations using the matched pair method. *N* – the number of collocated pairs; *STD* – standard deviation; *Q25* – lower quartile, 25% of the data lie below this value; *Q50* – median, 50% of the data lie below this value; *Q75* – upper quartile, 25% of the data lie above this value; *MB* – mean bias; *MAE* – mean absolute error; *RMSE* – root mean square error; *r* – Pearson's correlation coefficient score.

	WCL-Determined *SPH*	
	SPH^{top}	SPH^{ext}
MODIS-Terra/MAIAC		
N	163	
Lidar Observations Mean ± 1 *STD* (km)	2.162 ± 0.542	1.382 ± 0.368
Satellite Retrievals Mean ± 1 *STD* (km)	0.700 ± 0.550	
Lidar Observations $^{Max}/_{Min}$ (km)	$^{3.903}/_{1.254}$	$^{2.253}/_{0.800}$
Satellite Retrievals $^{Max}/_{Min}$ (km)	$^{2.650}/_{0.004}$	
Lidar Observations *Q25*, *Q50*, *Q75* (km)	1.776, 2.064, 2.508	1.131, 1.298, 1.581
Satellite Retrievals *Q25*, *Q50*, *Q75* (km)	0.325, 0.643, 0.952	
MB (km)	-1.462	-0. 683
MAE (km)	1.462	0.737
RMSE (km)	1.664	0.919
r	-0.055	0.146
MODIS-Aqua/MAIAC		
N	114	
Lidar Observations Mean ± 1 *STD* (km)	2.686 ± 0.797	1.790 ± 0.644
Satellite Retrievals Mean ± 1 *STD* (km)	0.370 ± 0.258	
Lidar Observations $^{Max}/_{Min}$ (km)	$^{4.215}/_{1.374}$	$^{3.422}/_{0.800}$
Satellite Retrievals $^{Max}/_{Min}$ (km)	$^{1.109}/_{0.025}$	
Lidar Observations *Q25*, *Q50*, *Q75* (km)	2.063, 2.627, 3.350	1.274, 1.728, 2.325
Satellite Retrievals *Q25*, *Q50*, *Q75* (km)	0.146, 0.308, 0.579	
MB (km)	-2.317	-1.419
MAE (km)	2.315	1.419
RMSE (km)	2.444	1.564

r	**0.220** *	0.148
MISR/MERLIN		
N	90	
Lidar Observations Mean ± 1 *STD* (km)	2.216 ± 0.506	1.498 ± 0.449
Satellite Retrievals Mean ± 1 *STD* (km)	2.114 ± 0.731	
Lidar Observations $^{Max}/_{Min}$ (km)	$^{2.982}/_{1.254}$	$^{2.253}/_{0.853}$
Satellite Retrievals $^{Max}/_{Min}$ (km)	$^{3.480}/_{0.625}$	
Lidar Observations *Q25*, *Q50*, *Q75* (km)	1.791, 2.204, 2.648	1.129, 1.428, 1.969
Satellite Retrievals *Q25*, *Q50*, *Q75* (km)	1.576, 1.965, 2.729	
MB (km)	-0.102	0. 616
MAE (km)	0.494	0.782
RMSE (km)	0.688	0.867
r	**0.444** **	**0.556** **
VIIRS/ASHE		
N	130	
Lidar Observations Mean ± 1 *STD* (km)	2.823 ± 0.999	1.895 ± 0.890
Satellite Retrievals Mean ± 1 *STD* (km)	2.707 ± 1.165	
Lidar Observations $^{Max}/_{Min}$ (km)	$^{5.493}/_{1.497}$	$^{4.003}/_{0.811}$
Satellite Retrievals $^{Max}/_{Min}$ (km)	$^{4.930}/_{0.231}$	
Lidar Observations *Q25*, *Q50*, *Q75* (km)	1.977, 2.904, 3.318	1.094, 1.629, 2.489
Satellite Retrievals *Q25*, *Q50*, *Q75* (km)	2.060, 2.683, 3.579	
MB (km)	-0.116	0.812
MAE (km)	1.190	1.594
RMSE (km)	1.697	1.806
r	**-0.220** *	**-0.220** *
TROPOMI/ALH		
N	127	
Lidar Observations Mean ± 1 *STD* (km)	2.677 ± 1.075	1.894 ± 0.936
Satellite Retrievals Mean ± 1 *STD* (km)	2.052 ± 0.588	
Lidar Observations $^{Max}/_{Min}$ (km)	$^{5.493}/_{1.374}$	$^{4.003}/_{0.734}$
Satellite Retrievals $^{Max}/_{Min}$ (km)	$^{3.425}/_{1.412}$	
Lidar Observations *Q25*, *Q50*, *Q75* (km)	1.718, 2.337, 3.308	1.019, 1.542, 2.684
Satellite Retrievals *Q25*, *Q50*, *Q75* (km)	1.546, 1.802, 2.431	
MB (km)	-0.625	0.158
MAE (km)	0.832	0.847
RMSE (km)	1.304	0.991
r	0.151	**0.241** **

*Note that the Pearson's correlation coefficient scores (r) in bold demonstrate a statistically significant relationship between the two variables; the symbol * signifies a p value < 0.05 and ** indicates a p value < 0.01. A lower p-value suggests a higher level of statistical significance.*

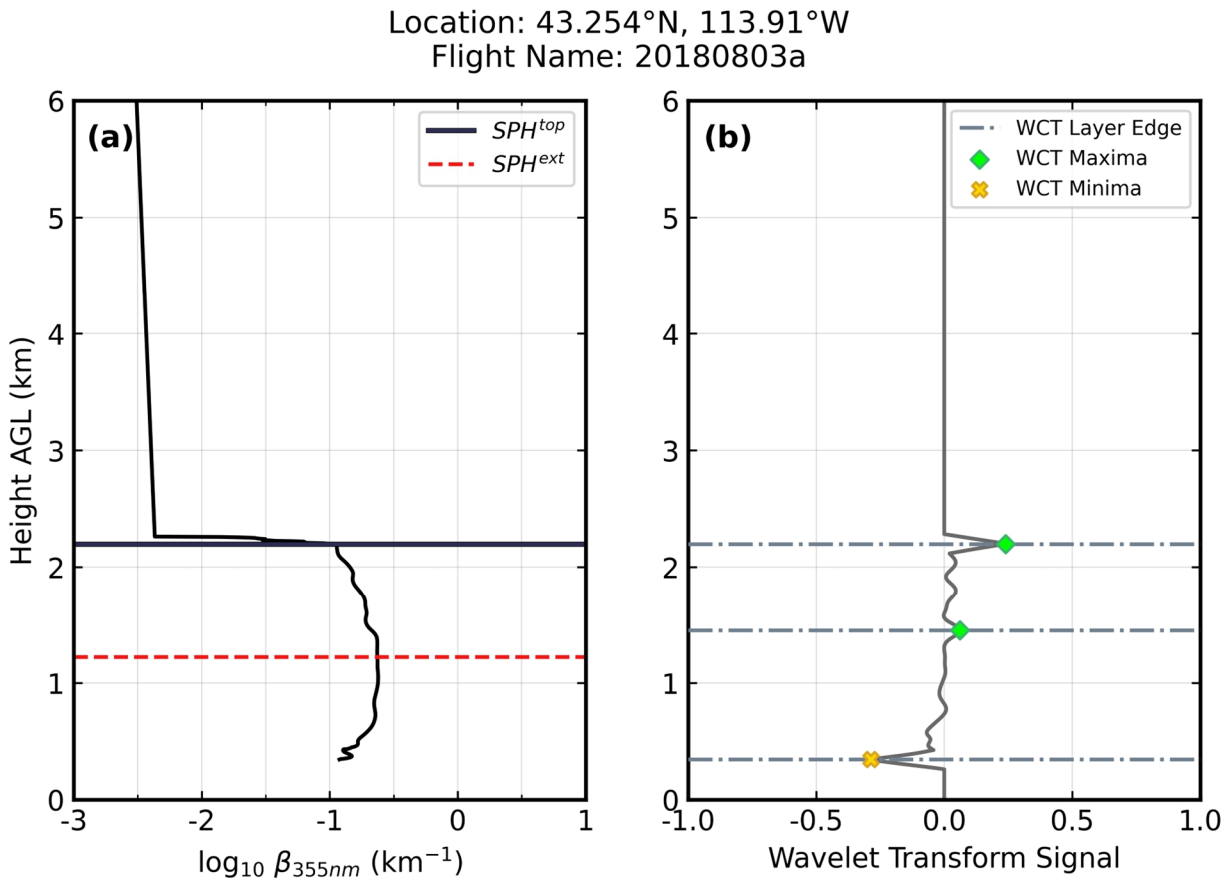

Figure S1: An example of a single-layered aerosol structure is presented here as evidenced by (a) the WCL aerosol extinction coefficient profile at 355 nm derived from the composite airborne lidar vertical cross-section and (b) the resulting WCT profile, on 3 August 2018 at a location (43.254° N, 113.91° W). In (a) the dashed red line represents the calculated SPH^{top}, while the calculated SPH^{ext} is shown as the solid blue line for comparison. In (b) the WCT-detected aerosol layer top (or bottom) is the horizontal dash-dotted grey line. The chromatic icons denote the local maxima (green, "diamond") and minima (yellow, "x") of the signal obtained through the WCT methodology.

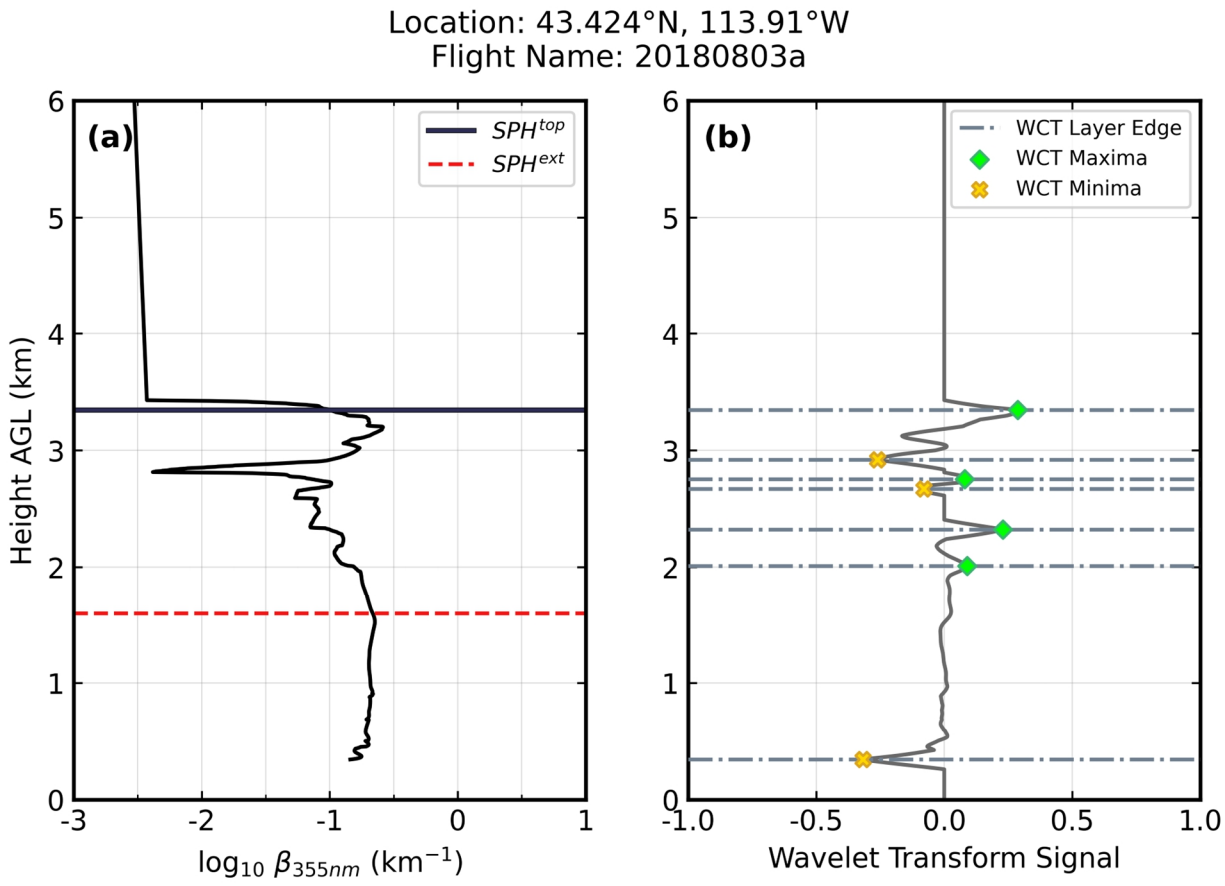

Figure S2: Another example has the same logic as shown in Figure S1, but for a multi-layered aerosol structure case on 3 August 2018 at a location (43.424° N, 113.91° W).

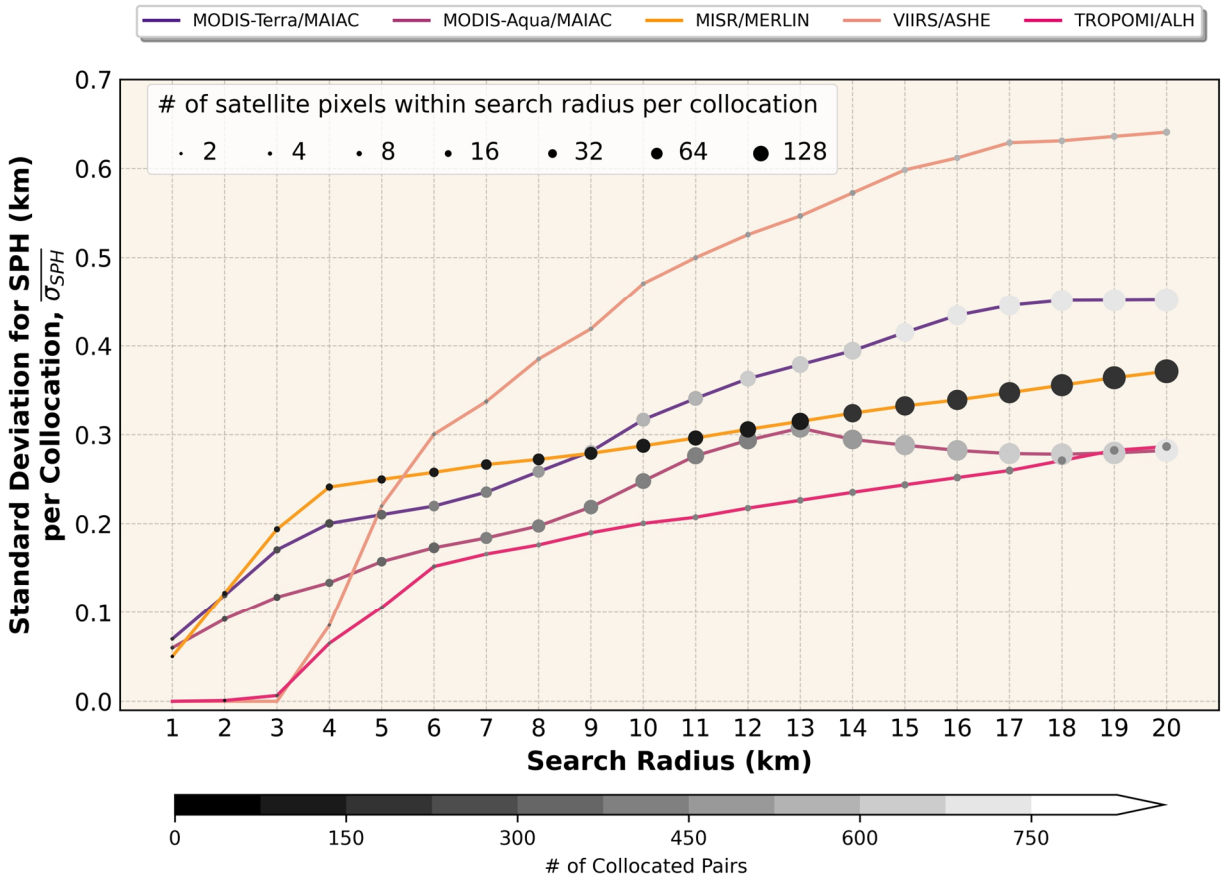

Figure S3: The *STD* for *SPH* per collocation of MODIS-Terra/MAIAC, MODIS-Aqua/MAIAC, MISR/MERLIN, VIIRS/ASHE, and TROPOMI/ALH as a function of search radius, for all successful collocations during the August 2018 BB-FLUX field campaign when the searching time window is set to 12 minutes. The color bar depicts the total number of collocation pairs between satellite and lidar observations. The larger the scatter point size, the greater the number of satellite pixels inside the circular area of a given search radius. A detailed workflow for the collocation methodology is demonstrated as follows. First, only those satellite pixels are picked that lie within the distance ranging from 1 km to 20 km and whose observation time is within 12 minutes from a given lidar point. From within this selected subset of satellite data, a nearest-neighbor search discovers one satellite pixel closest to the lidar point and the nearby satellite pixels inside the circular area of a certain search radius are also counted, if any. When that collocation is found, satellite-retrieved *SPH* value (AGL), lidar-determined *SPH* value (AGL), collocation's geolocations and associated satellite pixel counts in the sampling area around a lidar point are extracted and stored. Second, as seen in Figure SI.3, the search radius range will be narrowed down when the *STDs* of satellite-retrieved *SPH* products are above zero with a number of neighbors at least two. Finally, the best search radius is sorted based on the total collocation numbers but with a minimal value in satellite-retrieved *SPH* variations.

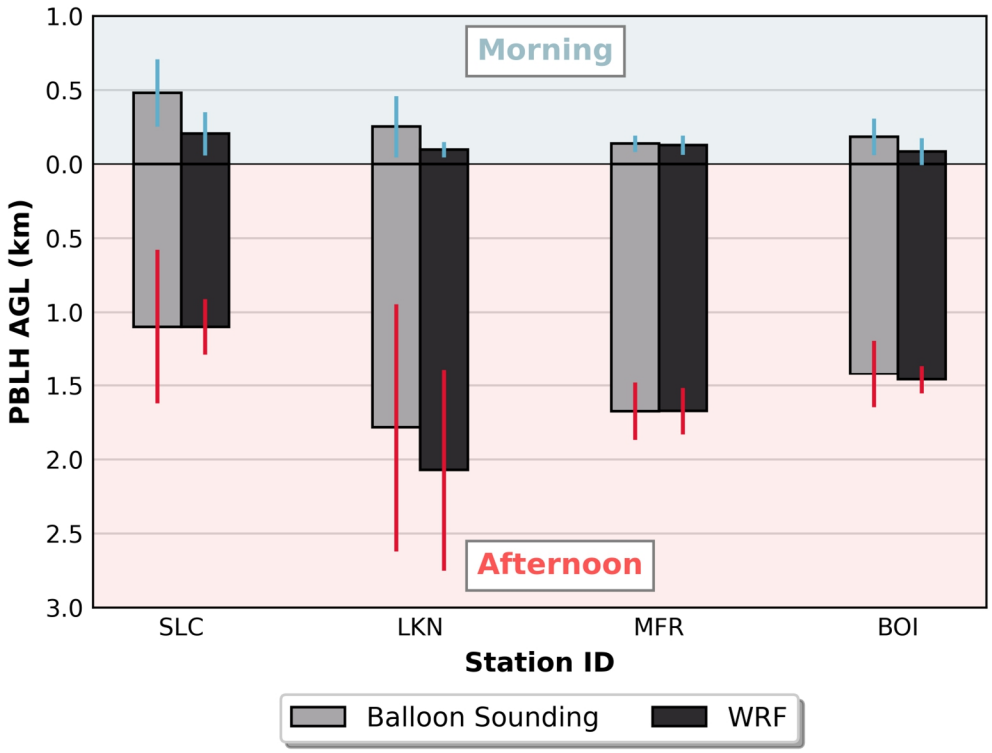

Figure S4: Diel averages (at 00Z-Afternoon and at 12Z-Morning, respectively) of *PBLH* with error bars derived from balloon soundings and WRF simulations during August 2018. Because there is uncertainty in the *PBLH* calculated in WRF these values are not used directly, but instead the PBL from WRF is calculated in the same manner as the balloon data, using the vertical potential temperature gradient method or the Richardson number method.

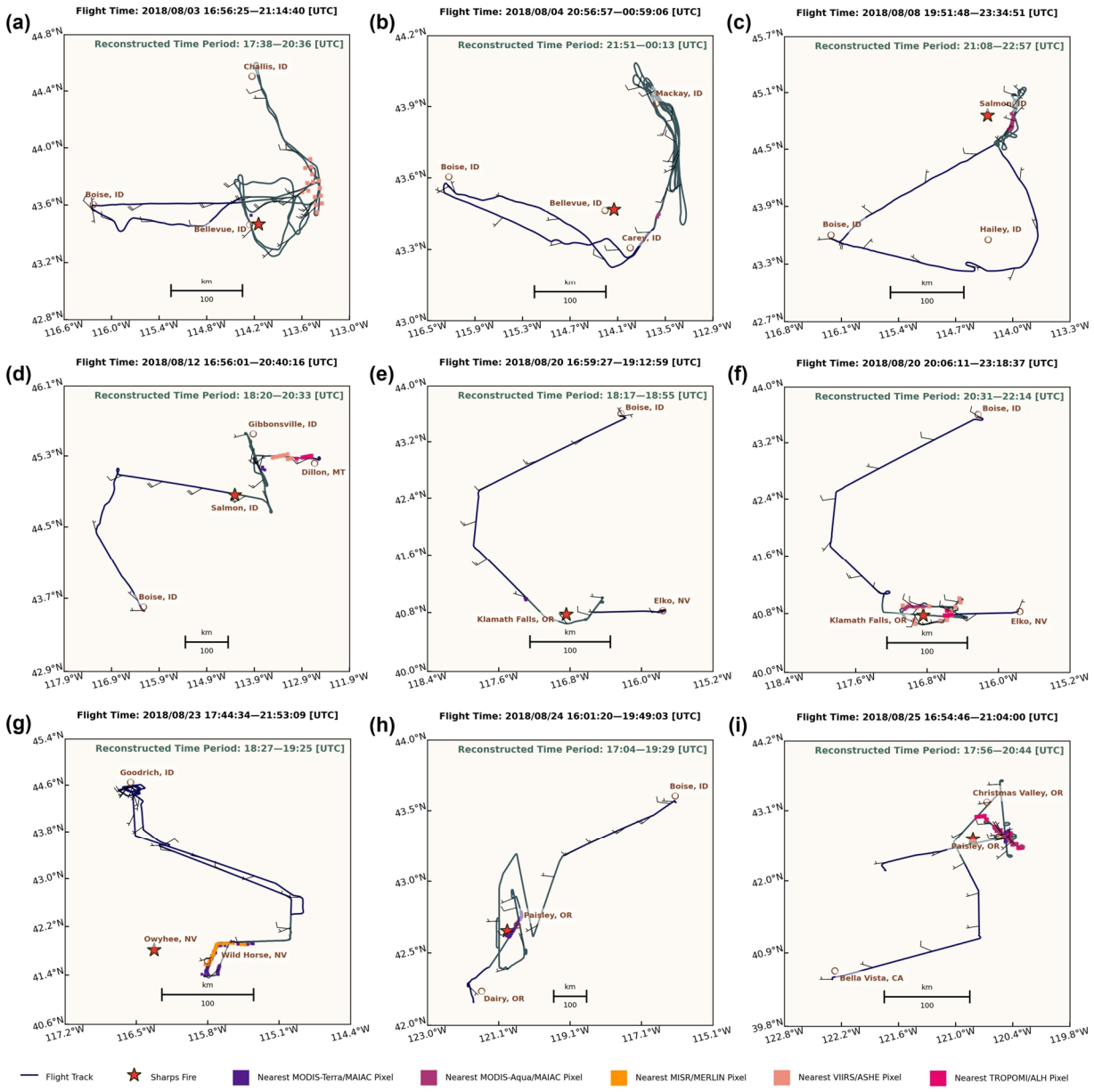

Figure S5: The other nine UWKA flight tracks selected from the August 2018 BB-FLUX campaign highlighted by reconstructed time periods are associated with four different kinds of satellite collocations: (a) 20180803a; (b) 20180804b; (c) 20180808b; (d) 20180812a; (e) 20180820a; (f) 20180820b; (g) 20180823a; (h) 20180824a; (i) 20180825a.

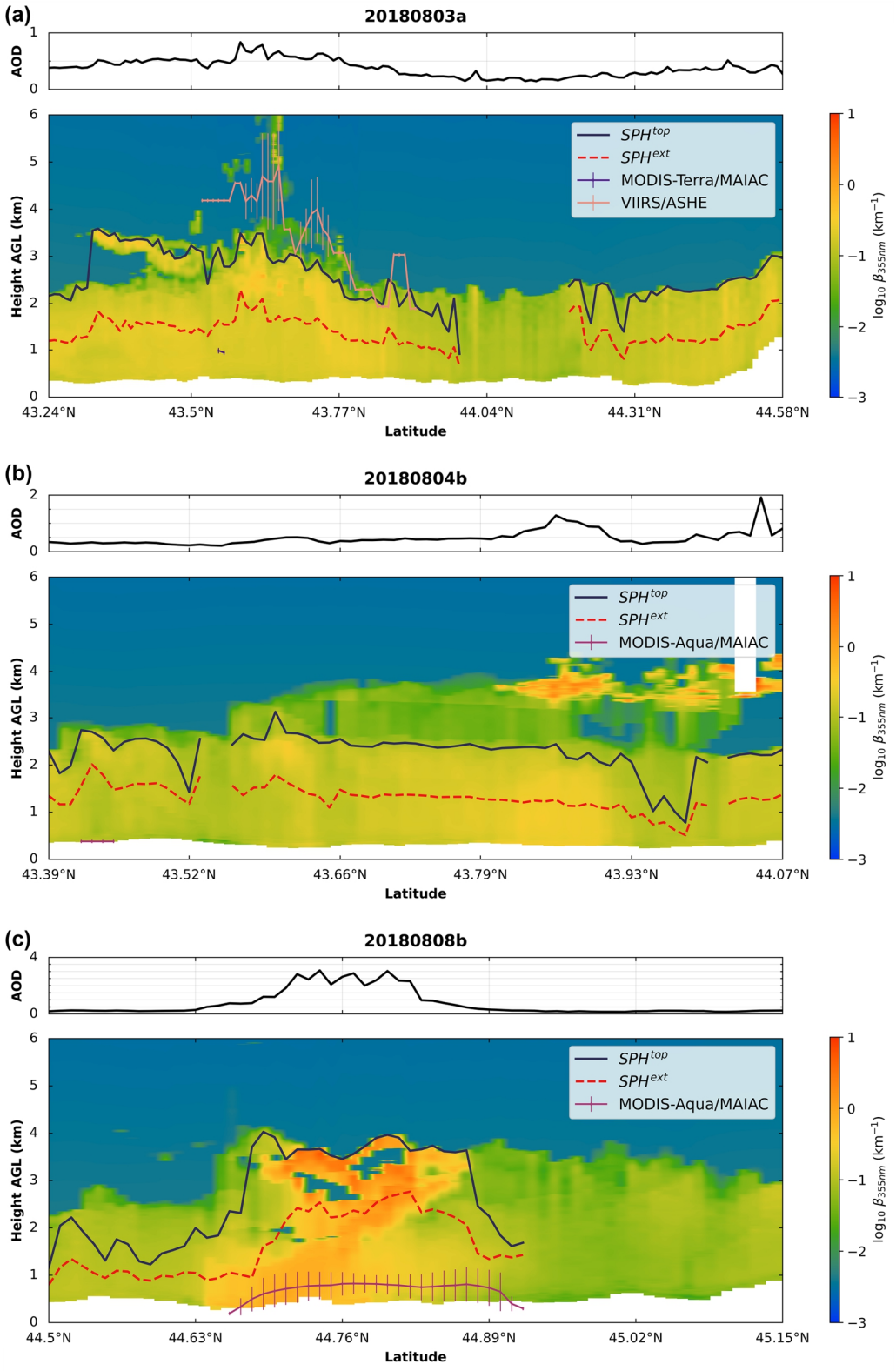

Figure S6: Cont.

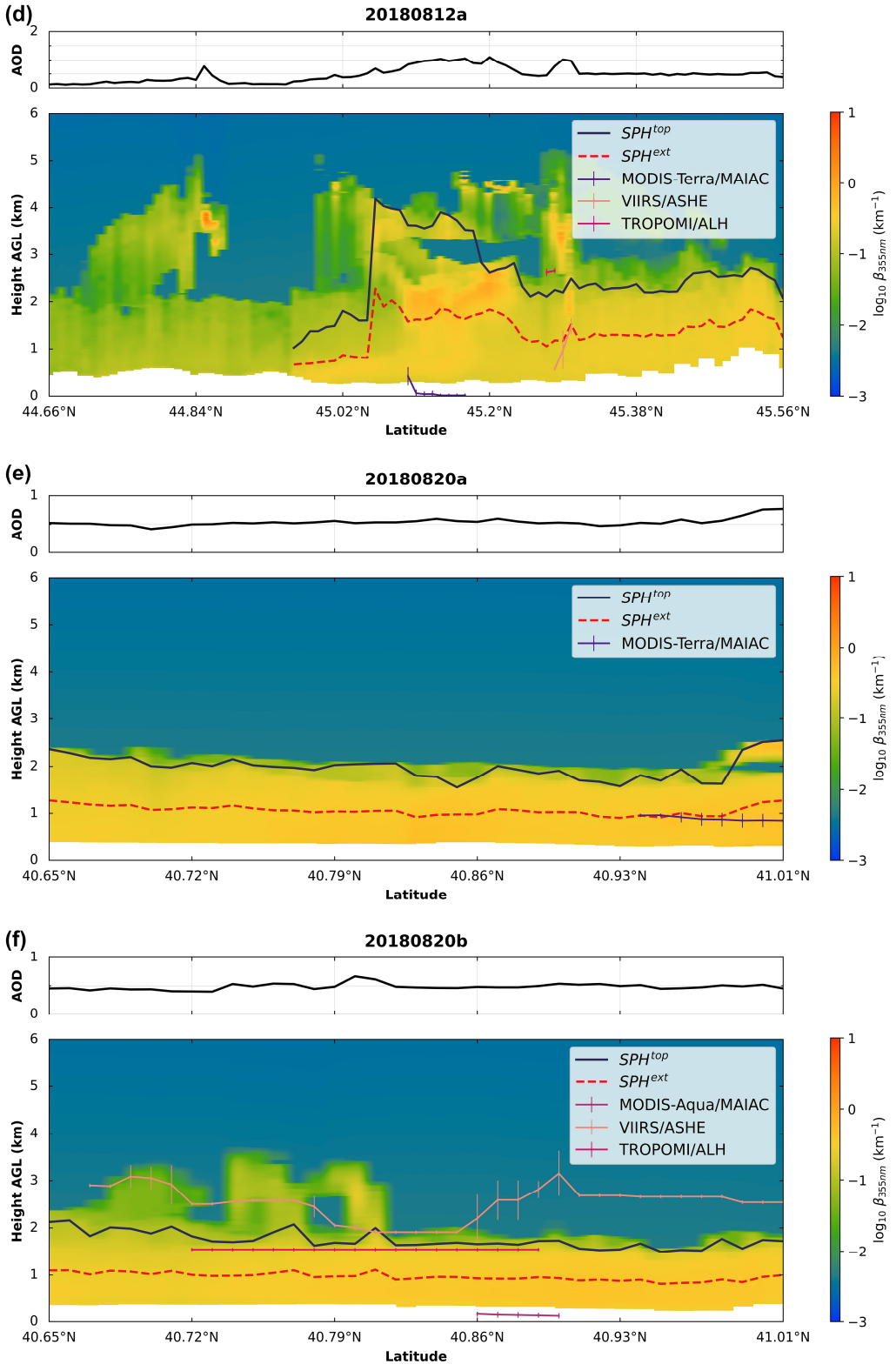

Figure S6: Cont.

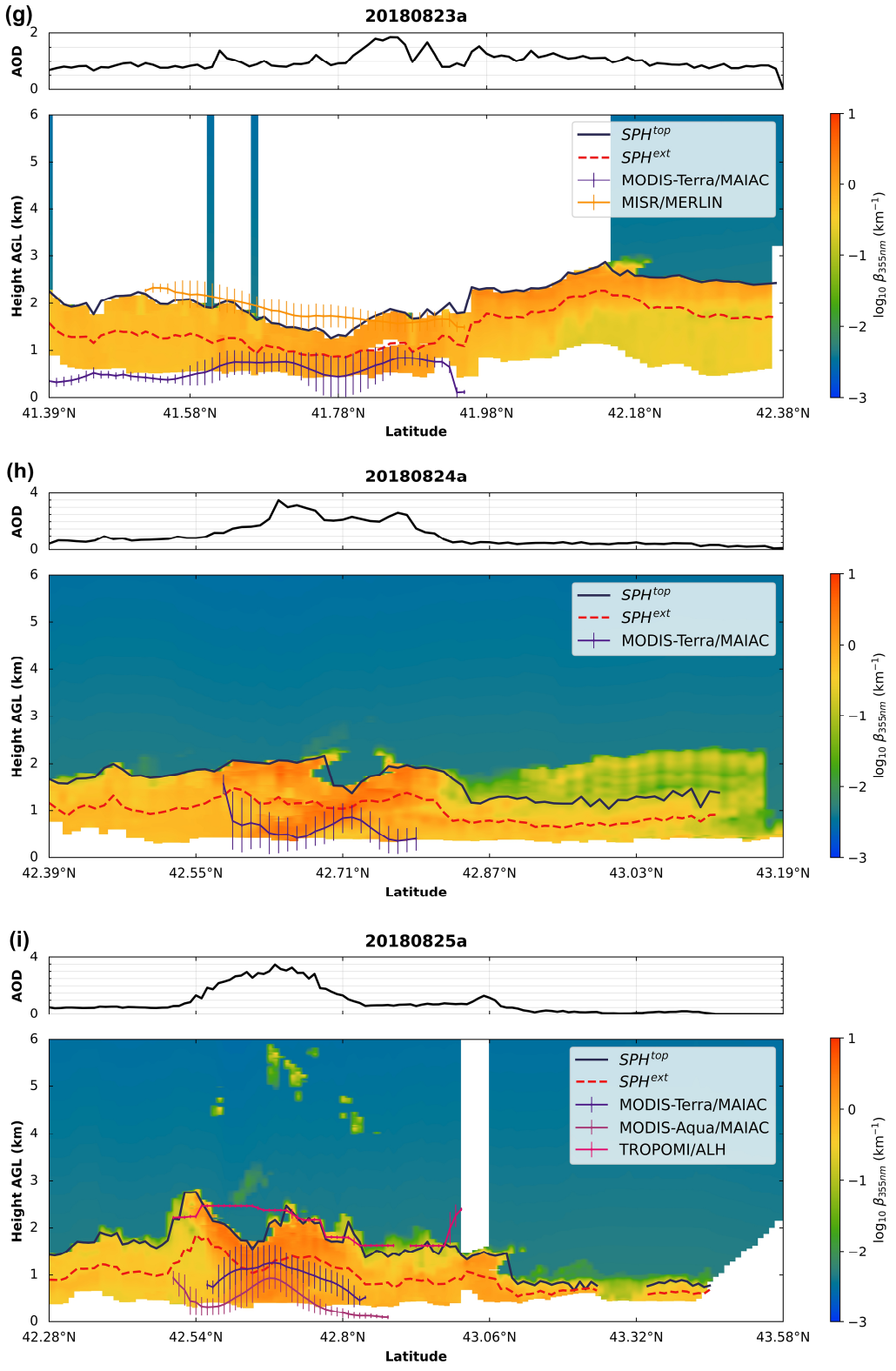

Figure S6: (Top panel) AOD variations at 355 nm along the eleven reconstructed flight tracks; (bottom panel) composite latitude-height cross-sections of WCL vertical aerosol extinction coefficient overlayed by WCL-determined *SPHs* (i.e., SPH^{top} and SPH^{ext}) as well as satellite-derived *SPHs* during the August 2018 BB-FLUX campaign: (a) 20180803a; (b) 20180804b; (c) 20180808b; (d) 20180812a; (e) 20180820a; (f) 20180820b; (g) 20180823a; (h) 20180824a; (i) 20180825a.

References

Chen, S.-H. and Sun, W.-Y.: A One-dimensional Time Dependent Cloud Model, Journal of the Meteorological Society of Japan, Ser. II, 80, 99–118, https://doi.org/10.2151/jmsj.80.99, 2002.

Grell, G. A. and Dévényi, D.: A generalized approach to parameterizing convection combining ensemble and data assimilation techniques, Geophys. Res. Lett., 29, 38–1, 2002.

Hong, S.-Y., Noh, Y., and Dudhia, J.: A new vertical diffusion package with an explicit treatment of entrainment processes, Mon. Weather Rev., 134, 2318–2341, 2006.

Iacono, M. J., Delamere, J. S., Mlawer, E. J., Shephard, M. W., Clough, S. A., and Collins, W. D.: Radiative forcing by long-lived greenhouse gases: Calculations with the AER radiative transfer models, J. Geophys. Res. Atmospheres, 113, 2008.

Jiménez, P. A., Dudhia, J., González-Rouco, J. F., Navarro, J., Montávez, J. P., and García-Bustamante, E.: A revised scheme for the WRF surface layer formulation, Mon. Weather Rev., 140, 898–918, 2012.

Tewari, M., Chen, F., Wang, W., Dudhia, J., LeMone, M., Mitchell, K., Ek, M., Gayno, G., and Wegiel, J.: Implementation and verification of the unified NOAH land surface model in the WRF model, Proceedings of the 20th conference on weather analysis and forecasting/16th conference on numerical weather prediction, Seattle, WA, USA, 2004.